

***c*-axis lattice dynamics in Bi-based cuprate superconductors**

N. N. Kovaleva,* A. V. Boris, T. Holden, C. Ulrich, B. Liang, C. T. Lin, B. Keimer, and C. Bernhard
Max-Planck-Institut für Festkörperforschung, Heisenbergstrasse 1, D-70569 Stuttgart, Germany

J. L. Tallon

McDiarmid Institute and Industrial Research Laboratory, Lower Hutt, New Zealand

D. Munzar

Institute of Condensed Matter Physics, Faculty of Science, Masaryk University, Kotlářská 2, CZ-61137 Brno, Czech Republic

A. M. Stoneham

University College London, London WC1E 6BT, United Kingdom

(Received 27 May 2003; revised manuscript received 16 October 2003; published 27 February 2004)

We present the results of a systematic study of the *c*-axis lattice dynamics in single-layer Bi₂Sr₂CuO₆ (Bi2201), bilayer Bi₂Sr₂CaCu₂O₈ (Bi2212), and trilayer Bi₂Sr₂Ca₂Cu₃O₁₀ (Bi2223) cuprate superconductors. Our study is based on both experimental data obtained by spectral ellipsometry on single crystals and theoretical calculations. The calculations are carried out within the framework of a classical shell model, which includes long-range Coulomb interactions and short-range interactions of the Buckingham form in a system of polarizable ions. Using the same set of shell model parameters for Bi2201, Bi2212, and Bi2223, we calculate the frequencies of the Brillouin-zone center phonon modes of A_{2u} symmetry and suggest the phonon mode eigenvector patterns. We achieve good agreement between the calculated A_{2u} eigenfrequencies and the experimental values of the *c*-axis TO phonon frequencies which allows us to make a reliable phonon mode assignment for all three Bi-based cuprate superconductors. We also present the results of our shell model calculations for the Γ -point A_{1g} symmetry modes in Bi2201, Bi2212, and Bi2223 and suggest an assignment that is based on published experimental Raman spectra. The superconductivity-induced phonon anomalies recently observed in the *c*-axis infrared and resonant Raman scattering spectra in trilayer Bi2223 are consistently explained with the suggested assignment.

DOI: 10.1103/PhysRevB.69.054511

PACS number(s): 74.72.Hs, 74.25.Kc, 78.20.Bh, 63.20.Dj

I. INTRODUCTION

The unusual *c*-axis charge transport in the cuprate high-*T_c* superconductors is still a subject of a controversial discussion. Of particular interest is a sizable absorption peak that develops below *T_c* in the far-infrared (FIR) range, accompanied with the strongly anomalous temperature dependence of some of the *c*-polarized IR phonon modes, in compounds that contain more than one CuO₂ plane per unit cell. Recently a reasonable description of these effects has been obtained with the so-called Josephson-superlattice model.¹⁻⁶ Here it is assumed that the individual CuO₂ planes are only weakly coupled by Josephson currents in the superconducting state. For bilayer compounds like YBa₂Cu₃O_{7- δ} (Y123) and Bi₂Sr₂CaCu₂O₈ (Bi2212) this results in two kinds of Josephson junctions with different longitudinal plasma frequencies, and their out-of-phase oscillation gives rise to a transverse Josephson plasma resonance, which has been assigned to the absorption peak that develops below *T_c*; the Josephson currents lead to a modification of the dynamical local electric fields and thus are at the heart of the observed phonon anomalies.^{2,4-6} The trilayer compounds provide an interesting testing ground for the various models that have been put forward to explain the unusual *c*-axis charge dynamics and the anomalous temperature dependence of some of the IR-active *c*-polarized phonon modes such as observed in the bilayer compounds. Indeed, a very recent experimental

study of the *c*-axis optical conductivity of a trilayer Bi₂Sr₂Ca₂Cu₃O₁₀ (Bi2223) provides clear evidence that the transverse Josephson plasma resonance is a universal feature of the multilayer high-*T_c* cuprate compounds.⁷ It has been shown that the Josephson-superlattice model^{2,4-6} allows a qualitative description of the transverse Josephson-plasma resonance and related phonon anomalies in Bi2223, which suggests that the Josephson currents lead to a strong variation of the dynamical local electric field even between the inner and outer CuO₂ planes of a trilayer.

The assignment of the IR-active *c*-polarized phonon modes and their polarization diagrams are of great importance for understanding these phenomena. While the properties of the IR-active phonon modes are indeed well known for the Y123 system,⁸⁻¹² the situation is not that clear for the bilayer high-*T_c* compounds of the type A₂Sr₂CaCu₂O₈ (A2212; A = Tl, Bi). Despite experimental^{5,6,13,14} and theoretical¹⁵⁻¹⁷ efforts, the assignment of the *c*-axis IR phonon modes in Bi2212 and Tl2212 remains contradictory, as discussed in Ref. 14. The situation is even less satisfactory for the trilayer high-*T_c* compounds A₂Sr₂Ca₂Cu₃O₁₀ (A2223) where the lack of single crystals of sufficient size and quality has inhibited detailed experimental investigations. Shell model calculations have been carried out for Tl2223 (Ref. 18) and IR measurements have been performed on ceramic samples of Tl2223 (Ref. 19) and more recently on oriented ceramics of Bi2223 (Ref. 20). The situation has

changed only very recently when some of the present authors managed to grow high-quality single crystals of the trilayer Bi compound $\text{Bi}_2\text{Sr}_2\text{Ca}_2\text{Cu}_3\text{O}_{10}$ that are suitable for IR measurements with light polarization along the c -axis direction.²¹

This paper reports a systematic investigation of the c -axis lattice dynamics of the bismuth-based compounds $\text{Bi}_2\text{Sr}_2\text{Ca}_{n-1}\text{Cu}_n\text{O}_{2n+4+d}$ that contain either $n=1, 2$, or 3 CuO_2 layers per unit cell. Our approach combines theoretical shell-model-based calculations with ellipsometric measurements of the c -axis dielectric response on well-characterized single crystals of high quality.^{21–23} From the ellipsometry experiments we obtain the frequencies of the c -axis-polarized IR-active phonon modes as well as the dielectric constants. On the theoretical side we model the Bi-based compounds with $n=1, 2$, and 3 in the $I4/mmm$ space group using the shell model approach, suggesting that screening due to free charge carriers should not have major effects.²⁴ This approach has been successfully applied to study lattice dynamics and various physical properties of high- T_c superconductors.^{15,18,25–27} The calculations have been performed using the GULP code.²⁸ The shell model parameters have been derived by fitting to the crystal structures in equilibrium as well as to experimental values of the dielectric constants and frequencies of the transverse optical (TO) phonon modes. Using the same set of shell model parameters for the $n=1, 2$, and 3 compounds we calculate the eigenfrequencies of the Brillouin-zone center phonon modes of A_{2u} symmetry and derive the phonon mode eigenvector patterns. Our results for the bilayer compound Bi2212 are consistent with those of the earlier shell model calculations in the $I4/mmm$ space group by Prade *et al.*¹⁵ We make an assignment of the c -axis-polarized phonon modes observed in the ellipsometric spectra of single-layer, bilayer, and trilayer Bi-based compounds by comparing with the calculated eigenfrequencies of A_{2u} symmetry modes. In addition, we also show the displacement patterns and calculated eigenfrequencies for the Raman-active phonon modes of A_{1g} symmetry according to the results of the present shell model calculations.

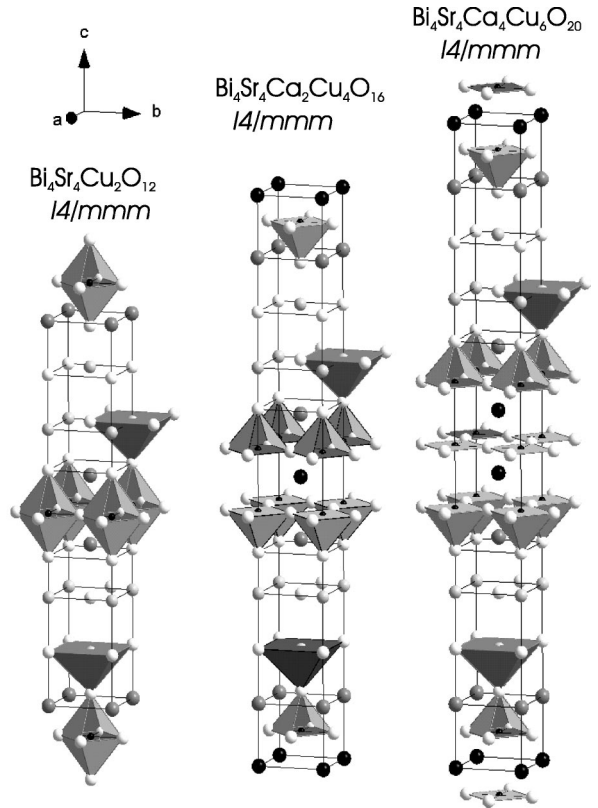


FIG. 1. Crystallographic cells of $\text{Bi}_2\text{Sr}_2\text{Ca}_{n-1}\text{Cu}_n\text{O}_{2n+4}$ with $n=1, 2$, and 3.

II. CRYSTAL STRUCTURE AND Γ -POINT PHONONS IN $\text{Bi}_2\text{Sr}_2\text{Ca}_{n-1}\text{Cu}_n\text{O}_{2n+4+\delta}$ WITH $n=1, 2$, AND 3

As a first approximation, a body-centered-tetragonal structure ($I4/mmm$) has been most frequently used in the interpretation of the IR and Raman spectra of Tl- and Bi-based compounds. According to the x-ray data,^{29,30} the three Bi-based cuprates of general formula $\text{Bi}_2\text{Sr}_2\text{Ca}_{n-1}\text{Cu}_n\text{O}_{2n+4+\delta}$ with $n=1, 2$, and 3 have similar structures of the tetragonal $I4/mmm$ space group (a_{tet}

TABLE I. The irreducible representations for the atoms in tetragonal $I4/mmm$ (D_{4h}^{17}) $\text{Bi}_2\text{Sr}_2\text{Cu}_6$ (Bi2201), $\text{Bi}_2\text{Sr}_2\text{CaCu}_2\text{O}_8$ (Bi2212), and $\text{Bi}_2\text{Sr}_2\text{Ca}_2\text{Cu}_3\text{O}_{10}$ (Bi2223).

Comp.	Atom	Wyc. not.	Site sym.	Irreducible	representation
Bi2201	Cu1	(1a)	D_{4h}	A_{2u}	$+E_u$
	Bi, Sr, O2, O3	(2e)	C_{4v}	$4(A_{2u}+A_{1g})$	$+E_g+E_u$
	O1	(2c)	D_{2h}	A_{2u}	$+B_{2u}+2E_u$
Bi2212	Ca	(1a)	D_{4h}	A_{2u}	$+E_u$
	Bi, Sr, Cu1, O2, O3	(2e)	C_{4v}	$5(A_{2u}+A_{1g})$	$+E_g+E_u$
	O1	(4g)	C_{2v}^v	$A_{2u}+A_{1g}+B_{1g}$	$+B_{2u}+2E_g+2E_u$
Bi2223	Cu2	(1a)	D_{4h}	A_{2u}	$+E_u$
	O4	(2c)	D_{2h}	A_{2u}	$+B_{2u}+2E_u$
	Bi, Sr, Ca, Cu1, O2, O3	(2e)	C_{4v}	$6(A_{2u}+A_{1g})$	$+E_g+E_u$
	O1	(4g)	C_{2v}^v	$A_{2u}+A_{1g}+B_{1g}$	$+B_{2u}+2E_g+2E_u$

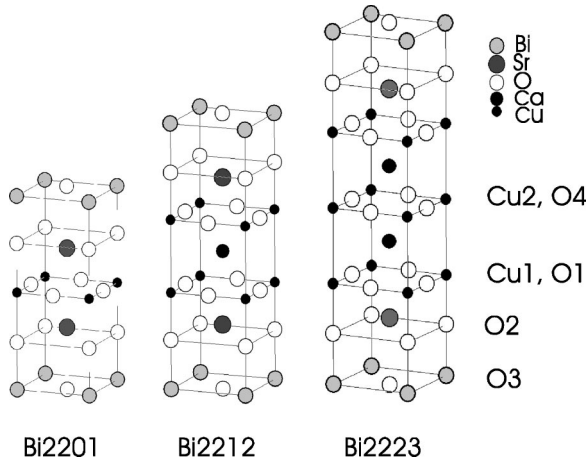


FIG. 2. Notations for copper and oxygen atoms in primitive unit cells of single-layer, bilayer, and trilayer Bi-based cuprates.

=3.814 Å), with two formula units (two primitive unit cells) in the crystallographic cell, as illustrated in Fig. 1. Primitive unit cells of single-layer, bilayer, and trilayer Bi-based cuprates differ only in the number ($n-1$) of $\text{CuO}_2\text{-Ca-CuO}_2$ slabs packed along the c axis; upon insertion of one and two slabs, the c axis parameter of the crystallographic cells increases from 24.6 to 30.6 and 37.1 Å (Ref. 30). The Wyckoff positions of the atoms and their site symmetries in tetragonal $I4/mmm$ (D_{4h}^{17}) primitive unit cells of $\text{Bi}_2\text{Sr}_2\text{CuO}_6$ (Bi2201), $\text{Bi}_2\text{Sr}_2\text{CaCu}_2\text{O}_8$ (Bi2212), and $\text{Bi}_2\text{Sr}_2\text{Ca}_2\text{Cu}_3\text{O}_{10}$ (Bi2223) are listed in Table I, with the notations of the atoms given in Fig. 2.

The irreducible representations corresponding to various atomic sites in the three Bi-based compounds that follow from the character tables of the point groups are presented in the right column of Table I. For the IR active modes at the Γ point of the Brillouin zone the displacement symmetries are

TABLE II. Mode classification from the irreducible representations for Bi2201, Bi2212, and Bi2223 in the tetragonal $I4/mmm$ (D_{4h}^{17}) space group.

Comp.	Γ_{IR}	Γ_{Raman}	$\Gamma_{acoustic}$	Γ_{silent}
Bi2201	$5A_{2u} + 6E_u$	$4A_{1g} + 4E_g$	$A_{2u} + E_u$	B_{2u}
Bi2212	$6A_{2u} + 7E_u$	$6A_{1g} + 7E_g + B_{1g}$	$A_{2u} + E_u$	B_{2u}
Bi2223	$8A_{2u} + 10E_u$	$7A_{1g} + 8E_g + B_{1g}$	$A_{2u} + E_u$	$2B_{2u}$

A_{2u} for a displacement in the z direction and E_u for displacements in the x or y direction, whereas those for the Raman-active Γ modes are A_{1g} , B_{1g} , and E_g , respectively. Due to full point-group symmetry of the Cu1 (Bi2201), Cu2 (Bi2223), and Ca (Bi2212) atoms with the $(1a)$ site position, no Raman-active modes of these atoms are allowed, and the three displacement vectors yield three modes of A_{2u} and E_u (doubly degenerate) character. The oxygen atoms in the mirror cuprate planes, O1 in single layer and O4 in trilayer Bi compounds, of D_{2h} -site symmetry, yield eigenmodes $A_{2u} + B_{2u} + 2E_u$. The in-plane oxygen O1 with C_{2v} -site symmetry in the bilayer and trilayer compounds generates eigenmodes $A_{2u} + A_{1g} + B_{1g} + B_{2u} + 2E_g + 2E_u$; among them, the B_{2u} mode is silent and E_g is doubly degenerated. The total numbers of modes grouped according to their optical activity in the three Bi-based compounds are summarized in Table II.

It has been shown that the actual structure of Bi-based compounds is better represented by orthorhombic $Cccm$ (D_{2h}^{20}) (Refs. 31–34) or $Ccc2$ (C_{2v}^{13}) (Refs. 35 and 36) space groups, most structural studies verify that the orthorhombic $Cccm$ structure is correct. To follow the consequences of the lowering symmetry it is convenient to use the $Amaa$ space group, which is a nonconventional setting of $Cccm$. The orthorhombic $Amaa$ structure has two formula units per primitive face-centered cell, with in-plane lattice parameters

TABLE III. The irreducible representations for the atoms in orthorhombic $Amaa$ (D_{2h}^{20}) $\text{Bi}_4\text{Sr}_4\text{Cu}_2\text{O}_{12}$ (Bi2201), and $\text{Bi}_4\text{Sr}_4\text{Ca}_2\text{Cu}_4\text{O}_{16}$ (Bi2212).

Comp.	Atom	Wyc. not.	Irreducible representations
Bi2201	Cu1	($2e$)	$A_u + 2B_{1u} + 2B_{2u} + B_{3u}$ $B_{1u} + B_{2u}$ tetragonal silent
	Bi, Sr, O2, O3	($4l$)	$4(A_u + 2B_{1u} + 2B_{2u} + B_{3u} + 2A_g + B_{1g} + B_{2g} + 2B_{3g})$ $4(B_{1u} + B_{2u} + A_g + B_{1g} + B_{3g})$ tetragonal silent
	O1	($4h$)	$A_u + B_{1u} + 2B_{2u} + 2B_{3u} + A_g + B_{1g} + 2B_{2g} + 2B_{3g}$ $A_g + B_{1g} + 2B_{2g} + 2B_{3g}$ tetragonal silent
Bi2212	Ca	($2e$)	$A_u + 2B_{1u} + 2B_{2u} + B_{3u}$ $B_{1u} + B_{2u}$ tetragonal silent
	Bi, Sr, Cu1, O2, O3	($4l$)	$5(A_u + 2B_{1u} + 2B_{2u} + B_{3u} + 2A_g + B_{1g} + B_{2g} + 2B_{3g})$ $5(B_{1u} + B_{2u} + A_g + B_{1g} + B_{3g})$ tetragonal silent
	O11, O12	($4h$)	$2(A_u + B_{1u} + 2B_{2u} + 2B_{3u} + A_g + B_{1g} + 2B_{2g} + 2B_{3g})$ $B_{1u} + 2B_{2u} + 2B_{3u} + A_g + B_{1g} + 2B_{2g} + 2B_{3g}$ tetragonal silent

TABLE IV. Mode classification from the irreducible representations for Bi2201 and Bi2212 in the orthorhombic *Amaa* space group.

Comp.	Γ_{IR}	Γ_{Raman}	$\Gamma_{acoustic}$	Γ_{silent}
Bi2201	$10B_{1u} + 11B_{2u} + 6B_{3u}$	$9A_g + 5B_{1g} + 6B_{2g} + 10B_{3g}$	$B_{1u} + B_{2u} + B_{3u}$	$6A_u$
Bi2212	$13B_{1u} + 15B_{2u} + 9B_{3u}$	$12A_g + 7B_{1g} + 9B_{2g} + 14B_{3g}$	$B_{1u} + B_{2u} + B_{3u}$	$8A_u$

a and b of approximately $a_{tet} \sqrt{2}$, and four formula units for the crystallographic cell, with the same c -axis parameter. By way of example, in the right column of Table III we present the irreducible representations corresponding to various atomic sites in the orthorhombic *Amaa* $\text{Bi}_4\text{Sr}_4\text{Cu}_2\text{O}_{12}$ (Bi2201) and $\text{Bi}_4\text{Sr}_4\text{Ca}_2\text{Cu}_4\text{O}_{16}$ (Bi2212) according to the structural data of Imai *et al.*,³¹ where we also show the modes which are silent in the tetragonal symmetry. The total numbers of modes grouped according to their optical activity in the *Amaa* Bi2201 and Bi2212 are summarized in Table IV. In Table V we show components of the IR- and Raman-active normal modes of the atoms with different Wyckoff positions at the Γ point of the Brillouin zone in the orthorhombic *Amaa* space group. From Tables I and III one can see that if the *I4/mmm* symmetry breaks down owing to the orthorhombic distortion of the structure, the degeneracy is removed. Thus, for each atom with ($2e$)-site position in the *I4/mmm* symmetry (Bi, Sr, O2, O3, and Cu1 in Bi2212) normal modes A_{2u} , A_{1g} , one E_u , and one E_g will become nondegenerate and, as a result, split into two; in addition, one new mode of B_{1g} character will appear in the orthorhombic *Amaa* structure. For the atoms Cu1 in Bi2201 and Ca in Bi2212 two new IR-active modes of B_{1u} and B_{2u} character are expected in the *Amaa* structure. Due to breaking of the tetragonal symmetry the O1 atom in Bi2201 will become ‘‘Raman active,’’ and, as a result, a number of Raman-active modes of A_g , B_{1g} , $2B_{2g}$, and $2B_{3g}$ character will appear.

However, it has been known that the actual structure of Bi-based cuprates is only pseudo-orthorhombic due to stacking faults, extra-stoichiometric oxygen, and incommensurate superstructural modulations along the b axis in BiO and SrO layers,³⁷ which result in substantial oxygen and cation disorder. These factors can yield additional phonon modes, in particular, ‘‘disorder-induced’’ modes. The crystal structure of Bi-based compounds therefore should be described in terms of a larger elementary cell and lower crystal symmetry. The origin of the superstructural incommensurate modulations of the atoms in BiO and SrO layers is not fully understood. The most common assumption is that the modulations are associated with extra-stoichiometric oxygen in the bilayer $\text{Bi}_2\text{O}_{2+\delta}$ that affects the orthorhombicity in the Bi-based cu-

prates. In this situation, whatever approximation, either tetragonal or orthorhombic, is adopted to make an assignment in the experimental phonon spectra, the first problem one has to solve is to distinguish the extra phonon modes—beyond the considered symmetry—due to the effects of superstructural incommensurate modulations and the presence of extra-stoichiometric oxygen in the Bi-based compounds.

Since the deviation from tetragonality in Bi-based compounds is not large, we suggest to start with the tetragonal *I4/mmm* approximation assuming that modes silent in tetragonal symmetry will be weak, and the simple tetragonal *I4/mmm* approximation should provide a useful first approximation for the assignment of the most intense IR- and Raman-active phonon modes. To explain more details in the experimental spectra due to possible orthorhombicity effects we suggest to invoke the group theory analysis based on the orthorhombic *Amaa* (D_{2h}^{20}) space group (see Table III).

III. SAMPLES AND EXPERIMENTAL TECHNIQUE

The Bi2201, Bi2212, and Bi2223 single crystals have been grown by the traveling solvent floating zone (TSFZ) method.^{21–23} The feed rods with nominal composition of $\text{Bi}_{2.1}\text{Sr}_{1.9}\text{Ca}_{n-1}\text{Cu}_n\text{O}_{2n+4+\delta}$ ($n = 1, 2$, and 3) were prepared by the conventional solid-state method. Slow growth rates of 0.5 and 0.2 mm/h were used for the Bi2201 and Bi2212 crystals, respectively. Since the Bi2223 crystallization field is the narrowest among the three members of the Bi-based family, an extremely slow growth rate of 0.04 mm/h was used. The Bi2201, Bi2212, and Bi2223 crystals were grown under applied oxygen pressure $p(\text{O}_2)$, in air, and in mixed gas flow of 80% Ar and 20% O_2 , respectively. Because of the significant difference between the lattice parameters of the a and b axes as compared to the one along the c axis, the growth rate is highly anisotropic and very slow along c . One typically obtains platelike crystals with large ab planes of about $6 \times 2 \text{ mm}^2$ but with much smaller dimensions along the c axis. The typical thickness is 1.5–2 mm for Bi2201, about 1 mm for Bi2212, less than 1 mm for Bi2223.

The crystals were characterized by energy dispersive x-ray (EDX) analysis, x-ray diffraction (XRD), transmission electron microscopy (TEM), and magnetic susceptibility and resistivity measurements. The as-grown Bi2212 crystals are phase pure with a pseudotetragonal structure; they are almost optimally doped with $T_c = 91 \text{ K}$ and $\Delta T_c = 2 \text{ K}$. The as-grown Bi2223 crystal contains 95%–98% of the Bi2223 pseudotetragonal phase with a minor fraction of layer-intercalated Bi2212. In the as-grown state the Bi2223 crystal was underdoped with $T_c = 97 \text{ K}$ (midpoint) and ΔT_c (10%–90% shielding fraction) = 7 K. After a post-annealing treat-

TABLE V. Components of normal modes of atoms with different Wyckoff positions in the orthorhombic *Amaa* space group.

Wyc. not.	A_g	A_u	B_{3g}	B_{3u}	B_{1g}	B_{1u}	B_{2g}	B_{2u}
(2e)		x		x		zy		yz
(4l)	zy	x	yz	x	x	zy	x	yz
(4h)	z	z	xy	xy	z	z	yx	yx

ment for 10 days in flowing oxygen at 500 °C with a subsequent rapid quenching to room temperature, the crystal became nearly optimally doped, with $T_c = 107$ K and $\Delta T_c = 3$ K. The undoped Bi2201 crystals grown by the TSFZ method are often nonsuperconducting. The superconductivity of the as-grown Bi2201 crystals is critically controlled by the oxygen content; therefore, the growth was carried out under oxygen pressures $p(\text{O}_2)$ ranging from 1 to 10 bars. The T_c of the as-grown Bi2201 crystals, determined from magnetic susceptibility measurements, varied between 3.5 and 8.5 K upon the Bi/Sr ratio and the oxygen pressure $p(\text{O}_2)$ applied in the course of growing. The structure of the as-grown Bi2201 crystals was determined to be pseudotetragonal; the lattice parameters were found to dependent upon the Bi/Sr ratio in the crystal composition. A pair of as-grown Bi2212 single crystals (taken from the same part of an ingot) was used for oxygen isotope replacement. The selected samples were annealed in isotopically enriched oxygen under identical conditions following a similar procedure described in Ref. 38.

For the ellipsometric measurements the crystal surfaces were polished to optical grade. The technique of ellipsometry provides significant advantages over conventional reflection methods in that (i) it is self-normalizing and does not require reference measurements and (ii) $\epsilon_1(\omega)$ and $\epsilon_2(\omega)$ are obtained directly without a Kramers-Kronig transformation (see Refs. 4 and 39 for a description of the technique). The ellipsometric measurements have been performed at the U4IR beamline of the National Synchrotron Light Source (NSLS) at Brookhaven National Laboratory and at the infrared beamline of the synchrotron radiation source ANKA at Karlsruhe Research Center, Germany. Homebuilt ellipsometers attached either to a Nicolet Magna 860 or a “Bruker” IFS 66v/S FT-IR spectrometer were used. The high brilliance of the synchrotron light source due to the small beam divergence enabled us to perform very accurate ellipsometric measurements in the far-IR range even on samples with comparably small ac faces.

IV. c-AXIS IR SPECTRA OF Bi2201, Bi2212, AND Bi2223 SINGLE CRYSTALS

Figure 3 shows the real parts of the c -axis optical conductivity $\sigma_1(\omega)$ and the dielectric function $\epsilon_1(\omega)$ at 150 K for the Bi2212 and Bi2223 single crystals with $T_c = 91$ K and $T_c = 107$ K. It is evident that the optical spectra look rather similar for both compounds. This is a consequence of the generic structural features of these two compounds. The electronic background is extremely weak and the spectra are dominated by the contributions of several IR-active phonon modes. Using the classical dispersion analysis we fit a set of Lorentzian oscillators simultaneously to $\epsilon_1(\omega)$ and $\epsilon_2(\omega)$ in the investigated spectral range. To describe the weak and rather flat electronic background in a Kramers-Kronig consistent way we have also included the sum of a Drude term and several very broad Lorentzian oscillators. As for the present purpose this description is rather formal we only limited the half-widths of the broad Lorentzians to values between 150 and 500 cm^{-1} . In Table VI we list the frequencies

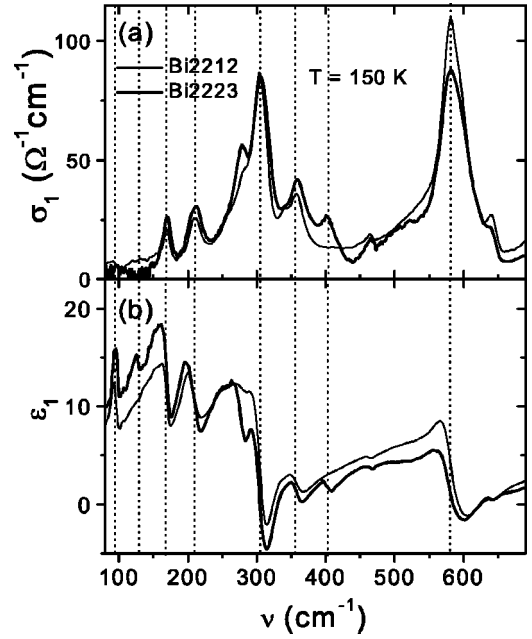


FIG. 3. Real parts of the c -axis (a) optical conductivity $\sigma_1(\omega)$ and (b) dielectric function $\epsilon_1(\omega)$ of Bi2212 and Bi2223 single crystals with $T_c = 91$ K and $T_c = 107$ K at $T = 150$ K.

$\omega_{\text{TO}j}$, oscillator strengths S_j , and damping parameters γ_j of the TO phonon bands observed in the $\epsilon_2(\omega)$ spectra of Bi2212 and Bi2223 single crystals, together with determined values of the high-frequency dielectric constants, ϵ_∞ .

For the Bi2223 we assign the main phonon bands at 97, 127, 170, 212, 305, 360, 402, and 582 cm^{-1} to the eight A_{2u} character modes. These modes are clearly identified especially due to the resonance features in $\epsilon_1(\omega)$ as shown in Fig. 3(b). Except for the two new intrinsic phonon modes in Bi2223 which appear at 127 and 402 cm^{-1} , the modes are observed at similar frequencies in both compounds. We believe that the remaining phonon features in Fig. 3 around 277, 466, and 640 cm^{-1} are beyond the tetragonal $I4/mmm$ approximation, as discussed in Sec. II. The feature at 640 cm^{-1} appears to be a weak satellite of the pronounced high-frequency mode at 583 cm^{-1} . It is likely related to the effects of characteristic incommensurate modulations which induce strong distortions in the SrO and BiO planes. Indeed, this feature almost disappears with Pb doping which significantly reduces these superstructural modulations.^{14,40} Concerning the mode at 277 cm^{-1} , on the low-frequency side of the pronounced band at 305 cm^{-1} , we find that its oscillator strength correlates with the amount of extra-stoichiometric oxygen that is incorporated within the $\text{Bi}_2\text{O}_{2+\delta}$ bilayer during the oxygen annealing treatment.⁷ By contrast with the 640- cm^{-1} satellite this feature remains persistent with Pb doping.⁴⁰ As a very weak feature at around 466 cm^{-1} is quite distant from the main phonon features we associate with the A_{2u} character modes, we would suggest that it is due to a contribution from some in-plane oxygen-related (O2 or O3) B_{2u} mode which has a $z(c)$ component (see Tables III and V) or it can be a “disorder-induced” defect mode.

The 150-K spectra of the real parts of the c -axis optical

TABLE VI. Frequencies $\omega_{\text{TO}j}$ (in cm^{-1}), oscillator strengths S_j , and damping parameters γ_j (in cm^{-1}) of the TO phonon bands observed in the c -polarized $\epsilon_2(\omega)$ spectra ($T=150$ K) of the single crystals Bi2201, Bi2212, and Bi2223. The assignment with the calculated frequencies of A_{2u} ($I4/mmm$) eigenmodes is given.

Bi2212				Bi2223				Bi2201			
$\omega_{\text{TO}j}$	S_j	γ_j	A_{2u}	$\omega_{\text{TO}j}$	S_j	γ_j	A_{2u}	$\omega_{\text{TO}j}$	S_j	γ_j	A_{2u}
97	–	–	93	97	–	–	88	109	0.56	5.00	77
–	–	–	–	127	0.10	9.1	145	–	–	–	–
168	0.29	8.7	195	170	0.63	11.2	211	165	0.45	12.3	175
210	0.34	12.7	304	212	0.77	21.4	252	208	0.65	14.5	–
282	0.16	12.3	–	277	0.50	17.4	–	–	–	–	–
304	1.13	21.7	343	305	1.43	27.6	335	301	1.31	24.7	293
358	0.33	30.7	403	360	0.46	30.7	378	385	0.85	25.2	353
–	–	–	–	402	0.16	24.0	516	–	–	–	–
462	0.02	10.5	–	466	0.02	10.5	–	–	–	–	–
521	0.22	85.3	–	512	0.26	81.0	–	501	0.10	48.0	–
583	0.65	38.2	643	582	0.61	41.9	666	586	0.42	31.2	596
640	0.03	17.8	–	640	0.03	17.8	–	639	0.01	12.5	–
$\epsilon_\infty=4.91$				$\epsilon_\infty=5.77$				$\epsilon_\infty=4.69$			

conductivity $\sigma_1(\omega)$ and dielectric function $\epsilon_1(\omega)$ of the as-grown nonsuperconducting Bi2201 single crystal, with the stoichiometric composition $\text{Bi}_2\text{Sr}_2\text{CuO}_6$, are shown in Fig. 4. The values of the fitted frequencies $\omega_{\text{TO}j}$, oscillator strengths S_j , and damping parameters γ_j of the TO phonon bands in the $\epsilon_2(\omega)$ are also listed in Table VI. To the best of our knowledge this is the first report of the c -polarized phonon spectra of the Bi2201 single crystal. Also we would like to note that the c -axis spectra of the Bi2201 reported here exhibit remarkable differences with respect to those of the isostructural single layer TI compound Tl2201 (Ref. 14). Six strong TO phonon features at around 109, 165, 208, 301,

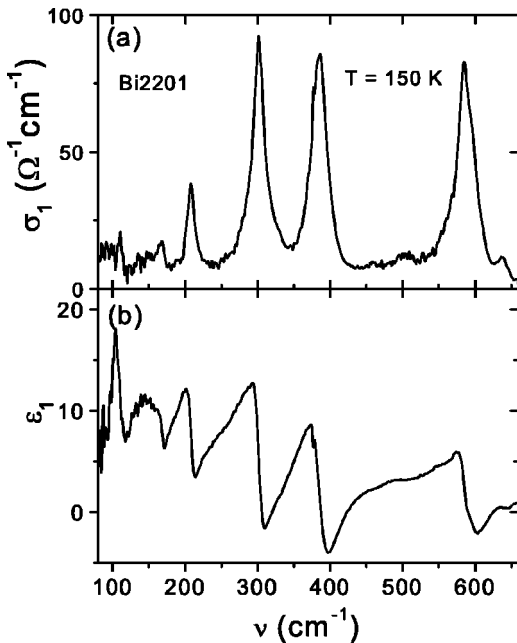


FIG. 4. c -axis (a) optical conductivity $\sigma_1(\omega)$ and (b) dielectric function $\epsilon_1(\omega)$ of Bi2201 single crystal at $T=150$ K.

385, and 586 cm^{-1} are clearly identified in the $\sigma_1(\omega)$ spectrum of Bi2201, as shown in Fig. 4(a), whereas only five A_{2u} character modes are expected from consideration in the ideal $I4/mmm$ space group (see Tables I and II). In addition to a weak satellite feature at around 640 cm^{-1} , which we have already discussed in the previous paragraph, one “extra” mode appears at low frequencies in the Bi2201. This presumably reflects that the deviation from the tetragonality is most pronounced for the single-layer Bi2201. We expect significant amplitudes in the c -polarized IR spectrum for the tetragonal forbidden B_{1u} mode of the Bi atoms, which are known to deviate most strongly from the tetragonal symmetry. We can also suggest that one new B_{1u} mode associated with the $(2e)$ site position of the Cu1 atoms in the A_{maa} Bi2201, which is tetragonally silent, can appear in the orthorhombic symmetry (see Table III). Also we have found that the spectra of superconducting Bi2201 crystals with T_c varying between 3.5 and 8.5 K depending on the Bi/Sr ratio and the oxygen stoichiometry exhibit almost the same phonon features.

We have furthermore investigated the oxygen isotope effect for ^{16}O and ^{18}O substitution in Bi2212 as shown in Fig. 5. For a mode with predominantly oxygen character the expected redshift of the eigenfrequency should be proportional to $[m(^{16}\text{O})/m(^{18}\text{O})]^{1/2} - 1$ —i.e., about 5.7%. A lower value of this so-called isotopic frequency shift signals that the corresponding phonon mode contains a significant contribution from the heavier (metal) ions. As shown in Fig. 5(a), a sizable redshift upon ^{18}O substitution is observed for the four A_{2u} phonons at 210, 304, 358, and 583 cm^{-1} ; the estimated values of the shifts are $8(\pm 1)$, $14(\pm 1)$, $19(\pm 1)$, and $32(\pm 1)$ cm^{-1} , respectively. This result confirms the expected trend that the three high-frequency modes at 304, 358, and 583 cm^{-1} have predominantly oxygen character. It is an interesting finding that the low-frequency mode at 210 cm^{-1} also exhibits a sizable redshift, which suggests that it con-

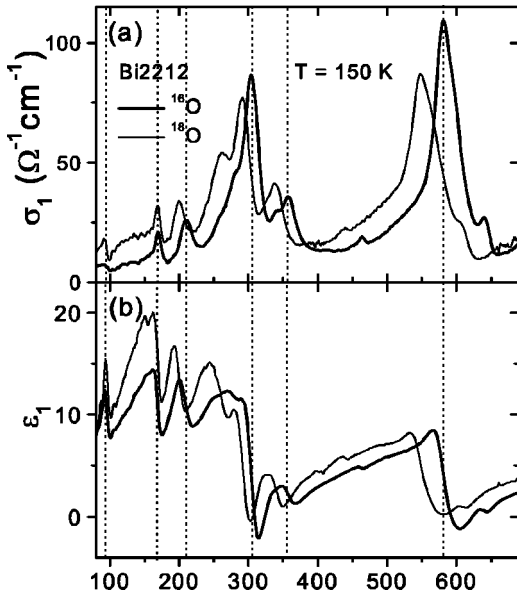


FIG. 5. Oxygen isotope effect in the c -polarized response of (a) $\sigma_1(\omega)$ and (b) $\epsilon_1(\omega)$ of Bi2212 with $T_c=91$ K, measured at 150 K.

tains a significant contribution from the oxygen vibrations. Some of the c -polarized IR phonon modes in the bilayer Bi2212 and trilayer Bi2223 compounds exhibit a strongly anomalous temperature dependence at T_c that is accompanied by the development of a sizable absorption peak below T_c in the FIR range.^{2,5-7} Figures 6(a) and 6(b) show the real part $\sigma_1(\omega)$ of the c -axis optical conductivity of Bi2212 and Bi2223 at two different temperatures, above T_c and well below T_c . In the normal state the spectra exhibit hardly any noticeable changes, except for a sharpening of the phonons with decreasing temperature. Right below T_c , however, the spectra change appreciably. This is also illustrated in Fig. 6(c) which displays the difference $\sigma_1(T \ll T_c, \omega) - \sigma_1(T \gg T_c, \omega)$. The most prominent feature is the broad absorption band around 500–550 cm^{-1} which appears below T_c and grows rapidly with decreasing temperature. This absorption band has been identified in both Bi2212 and Bi2223 and has been attributed to the transverse Josephson-plasma resonance (t-JPR) that is a universal feature of the multilayer high- T_c cuprate compounds.^{2,4,6} It is evident from Fig. 6 that the formation of the t-JPR is associated with an anomalous temperature dependence of the phonon modes at 360, 402 (specific for trilayer Bi2223), and 582 cm^{-1} denoted by A, B, and C in Fig. 6. The principal difference between the phonon anomalies observed in the bilayer and trilayer Bi systems at T_c is that in the latter system the changes of the spectral weight of the apical phonon mode are much more pronounced and an additional phonon mode exhibiting the opposite temperature dependence is observed at 402 cm^{-1} .

V. THEORETICAL CALCULATIONS

A. Shell model approximation and potential parameters

To estimate the frequencies at which the various eigenmodes appear and, consequently, to make the assignment in

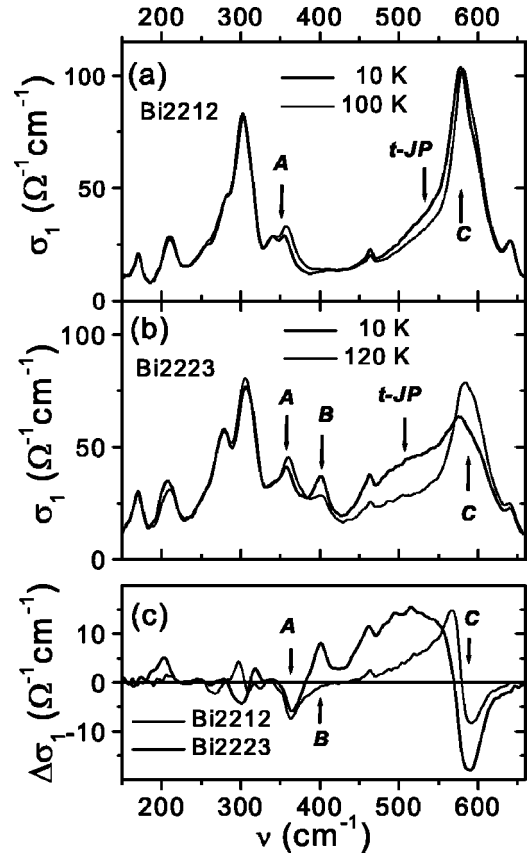


FIG. 6. Real part $\sigma_1(\omega)$ of the FIR c -axis conductivity (a) of Bi2212 with $T_c=91$ K for $T=100$ K and $T=10$ K (Ref. 6) and (b) of Bi2223 with $T_c=102$ K for $T=120$ K and $T=10$ K (Ref. 7). (c) Superconductivity-induced changes of the FIR conductivity, $\Delta\sigma_1 = \sigma_1(T \leq T_c, \omega) - \sigma_1(T \geq T_c, \omega)$, for Bi2212 and Bi2223 derived from the data shown in the top panels. The most pronounced phonon anomalies are denoted by A, B, and C.

the experimental phonon spectra (at $T=150$ K), we have performed lattice-dynamical calculations using the shell model approximation. We performed the calculations for the three Bi-based structures Bi2201, Bi2212, and Bi2223 within the ideal tetragonal $I4/mmm$ (D_{4h}^{17}) space group, using the lattice constants and internal z structural parameters reported in Refs. 29 and 30. We apply the shell model approach suggesting that screening due to free charge carriers should not have major effects.^{24,41} Earlier the shell model approach was successfully applied to study lattice dynamics and various physical properties of high- T_c superconductors.^{15,18,25-27} Our calculations are performed using the GULP code.²⁸ In the context of the shell model, the lattice is considered as an assembly of polarizable ions, represented by massive point cores and massless shells coupled by isotropic harmonic forces. The interaction includes contributions from Coulomb and short-range interactions. Short-range interactions between relatively small cations are usually ignored. The core and shell charges and the spring constant of each ion are parameters of the model. The short-range potentials used for the shell-shell interactions are of the Buckingham form

$$V_{ij} = A_{ij} \exp(-r/\rho_{ij}) - C_{ij}/r^6. \quad (1)$$

The Buckingham potential parameters as well as the atoms' core and shell charges and the relevant spring constants were fitted in this work. To obtain a self-consistent set of the shell model parameters acceptable for a family of Bi-based high- T_c cuprates, we performed fits simultaneously to the structures of Bi2201, Bi2212, and Bi2223. As the starting values for the shell model parameters—pair potentials, net ionic charges, shell and core charges, and relevant spring constants—we used the ones obtained by Baetzold for a bilayer cuprate $\text{YBa}_2\text{Cu}_3\text{O}_{7-\delta}$ system within the similar CASCADE code.²⁶ We have two reasons to keep the net ionic charges of the atoms in the cuprate planes of $+2|e|$ for Cu1 and Cu2 and $-2|e|$ for O1 and O4. First, it is in line with the approach of Baetzold for Y123 (Ref. 26) and, second, this is required if we want to describe single-layer, bilayer, and trilayer Bi systems by the same set of potential parameters. Otherwise, by dividing the noninteger charges between the cuprate planes we would have different pair potential parameters in each case. Following the approach of Baetzold, we also keep the same effective charges of $-1.67|e|$ for O2 and O3. We take the formal ionic charge $+2|e|$ for Sr, and to satisfy the electroneutrality conditions we have to assume an effective charge $+2.33|e|$ for Bi. The formal charges here describe the dipole moment per unit displacement, rather than the charge within some region of space. It was noted by Catlow and Stoneham that even the integer charge-distribution method can be successfully employed to accurately calculate physical properties of solids where ionicity may vary over a range of values.⁴² We assume a shell charge of $-3.2576|e|$ for all oxygen ions, as in Ref. 26. The Sr, Bi, Ca, and O ions are treated as polarizable, while the Cu ions are treated as unpolarizable. The fitting procedure keeps O-O (shell-shell) interactions as those of typical oxides.^{43,44} The structures were allowed to relax to equilibrium conditions under the symmetry ($I4/mmm$) restrictions; the cores and shells were allowed to move separately. The forces on the atoms were minimized by varying the potential parameters; the eigenvalues for the first three modes for all three compounds had approximately zero values, indicating a stable structure in each case. Normally a good fit requires some information on physical properties—elastic, dielectric, and piezoelectric (where applicable) constants—as well as the structure. In general, vibrational frequencies contain far more information than any of the above. However, in fitting the frequencies a reasonable implication for the assignment as to be suggested, at least for some key modes. In the present work a final fit was done to the available experimental data on the bilayer Bi2212 compound. The criterion of a successful fit was good agreement with the structural parameters,²⁹ provided that approximately zero forces are applied for all atoms, with the c axis static ϵ_0 and high-frequency ϵ_∞ dielectric constants and with the frequencies of the c -axis IR- and Raman-active optical phonons.⁴⁵ The resulting Buckingham potential parameters, ionic shell charges (Y), and force constants (k) are presented in Table VII. To simulate different in-plane and out-of-plane bond lengths in the structures of Bi-based compounds, as well as the anisotropy of oxygen polarizability, generally we have arrived at different pair potentials for the Cu-O, Sr-O, and Bi-O in-plane and out-of-

plane short-range interactions. It is particularly remarkable that the pair potentials for the Bi-O2 and Bi-O3 short-range interactions are significantly different, and this fact seems to be mainly due to very different Bi-O bond lengths; i.e., in the structures of Bi-based compounds we have a Bi-O2 bond length of 2.22 Å, an in-plane Bi-O3 bond length of 2.71 Å, and the longest Bi-O3 bond length, between weakly coupled Bi_2O_2 biplanes, of 2.97 Å (Ref. 29). Thus elaborated, our shell model parameters allow us to describe all three Bi-based structures by the same set of short-range pair-potential parameters, listed in Table VII. To compare the experimental and calculated structures we present experimental values of the fractional atomic coordinates obtained from Refs. 29 and 30 and the corresponding calculated values in Table VIII, where we also show the experimental errors for the Bi2212 fractional coordinates²⁹ in brackets. As far as our final fit is based on the Bi2212 crystal, the best agreement with the internal structural parameters is naturally obtained for this system. As can be seen from Table VIII these parameters reproduce also reasonably well the Bi2223 and Bi2201 structures. Slightly varying the shell model parameters we can arrive at a better agreement with the particular structure chosen, although we would rather aim to obtain a self-consistent set of shell model parameters, which can account for the common generic features in all three Bi-based structures. Going ahead, we would like to mention here that this would not qualitatively affect the character of the eigenmodes resulting from our shell model calculations, although the eigenfrequencies and amplitudes of the eigenvectors of the c -axis phonon modes can slightly change. The elastic properties calculated with these parameters do not exhibit unphysical (i.e., negative) values, and the eigenvalues for the first three modes have approximately zero values in all three compounds which is indicative of a stable structure. We have also arrived at a good agreement with the experimental values for dielectric constants. All three compounds Bi2212, Bi2223, and Bi2201 have close values of c -axis dielectric constants within the range $\epsilon_0 \approx 9.5\text{--}12.0$ and $\epsilon_\infty \approx 4.9\text{--}5.8$, as estimated from our experimental $\epsilon_1(\omega)$ and $\epsilon_2(\omega)$ spectra. The corresponding calculated values fall in the range $\epsilon_0 \approx 10.9\text{--}13.9$ and $\epsilon_\infty \approx 4.8\text{--}5.6$. Certainly, the obtained set of shell mode parameters is not unique. Nevertheless, given the fact that by using the same set of parameters we can reproduce the structures and main phonon bands as observed for all three compounds we obtain more confidence in the assignment for the phonon modes.

B. Calculated Γ -point A_{2u} symmetry modes in Bi2201, Bi2212, and Bi2223

In Fig. 7 we show the eigenvector patterns corresponding to six eigenmodes of A_{2u} symmetry and one silent mode of B_{2u} symmetry for Bi2212, resulting from our lattice-dynamical calculations. Under each patch we list values of the eigenfrequencies and below we make an assignment based on a comparison with the experimental frequencies of the TO phonon bands observed in the c -polarized spectra of the Bi2212 single crystal ($T=150$ K, see Fig. 3 and Table VI). Mixing due to out-of-phase motion of ions of equal

TABLE VII. Potential parameters for short-range shell-shell interactions [Eq. (1)], ion shell charges (Y), and force constants (k) in tetragonal $I4/mmm$ (D_{4h}^{17}) $\text{Bi}_2\text{Sr}_2\text{CuO}_6$, $\text{Bi}_2\text{Sr}_2\text{CaCu}_2\text{O}_8$, and $\text{Bi}_2\text{Sr}_2\text{Ca}_2\text{Cu}_3\text{O}_{10}$; in-plane O1 and O4 oxygen ions are taken of a net charge $-2.0|e|$; out-of-plane O2 and O3 oxygen ions are taken of a net charge $-1.67|e|$, $r_{\text{cutoff}}=99 \text{ \AA}$.

	A (eV)	ρ (\AA)	C (eV \AA^{-6})
Cu1-O1; Cu2-O4	3889.8	0.24273	0.00
Cu1-O2,O4; Cu2-O1	2708.0	0.22074	0.00
Ca-O1; Ca-O4	14882.2	0.24203	0.00
Sr-O1	1487.9	0.33583	0.00
Sr-O2	20097.2	0.24823	0.00
Sr-O3	30202.0	0.24823	0.00
Bi-O2	15671.0	0.22074	0.00
Bi-O3	147997.9	0.22074	0.00
Cu1-Sr	167925.4	0.22873	0.00
Sr-Sr	3680.5	0.25880	0.00
Sr-Bi	158000.0	0.22873	0.00
Bi-Bi	7100.0	0.22873	0.00
Ca-Ca	4500.0	0.22873	0.00
O-O	22764.0	0.14900	75.00

Ion	$Y(e)$	k (eV \AA^{-2})
Ca	2.00	99.0
Cu1, Cu2	2.00	999999.0
Bi	2.33334	27.2
Sr	5.09995	146.7
O1	-3.25760	26.0
O4	-3.25760	76.0
O2, O3	-3.25760	100.0

symmetry in inequivalent positions often does not allow the determination of a unique character for a given set of equal symmetry modes. The total number of the modes in each symmetry, of course, is unaffected by mixing. The character of the assigned modes is determined according to the dominant contribution from the atoms participating in the vibration and shown atop. The respective calculated components

TABLE VIII. A comparison between the experimental and calculated structures of Bi2212, Bi2223, and Bi2201 [$I4/mmm$ (D_{4h}^{17})]. Experimental values of the fractional atomic coordinates and corresponding calculated values are given, with the experimental errors for Bi2212 structure shown in brackets.

	Bi2212		Bi2223		Bi2201	
	z , expt.	z , calc.	z , expt.	z , calc.	z , expt.	z , calc.
Ca	0.00	0.00	0.0443	0.0464	-	-
Sr	0.1097(5)	0.1096	0.1346	0.1369	0.0759	0.0696
Bi	0.3022(3)	0.3043	0.292	0.297	0.3148	0.3175
Cu1	0.4456(9)	0.4334	0.4109	0.4010	0.00	0.00
Cu2	-	-	0.00	0.00	-	-
O1	0.446(3)	0.445	0.411	0.408	0.00	0.00
O2	0.375(4)	0.372	0.353	0.352	0.405	0.401
O3	0.205(4)	0.211	0.213	0.219	0.194	0.201
O4	-	-	0.00	0.00	-	-

of the eigenvector amplitudes are given in Table IX. The lowest-frequency mode calculated at 93 cm^{-1} (experimentally observed at 97 cm^{-1} ; see Fig. 3 and Ref. 5) is related to motion of the heavy Bi atoms, which is strongly mixed with out-of-phase motion of Sr, Cu1, and Ca, with a small oxygen contribution from different crystallographic planes. The next mode of A_{2u} symmetry calculated at 195 cm^{-1} (168 cm^{-1}) is predominantly due to motion of the Cu1 against Sr, with a small contribution from the Ca ions. The A_{2u} mode at 304 cm^{-1} (210 cm^{-1}) is due to the vibrations of Ca and O1 ions against Sr and O3. This mixed low-frequency mode contains a noticeable contribution from the copper-plane O1 ions and bismuth-plane O3 ions to the c -axis oscillations. The three high-energy vibrations are predominantly oxygen related. The mode calculated at 343 cm^{-1} (304 cm^{-1}) is basically due to O3 and O1 vibrations against Sr and Ca atoms, with a predominant contribution from the bismuth-plane oxygen O3. The Cu-O bond-bending character mode at 403 cm^{-1} (358 cm^{-1}) involves a significant contribution from the copper-plane O1 ions, vibrating against the Ca and O3 atoms. The highest-frequency mode at 643 cm^{-1} (583 cm^{-1}) is due to O2 and O3 out-of-phase oscillations, and it has apparently apical character due to a predominant contribution from the strontium-plane O2 oscillations along the c axis. Our assignment and the eigenvectors for the c -polarized phonon modes can be tested by the oxygen iso-

Infrared A_{2u} (Bi2212 $I4/mmm$)

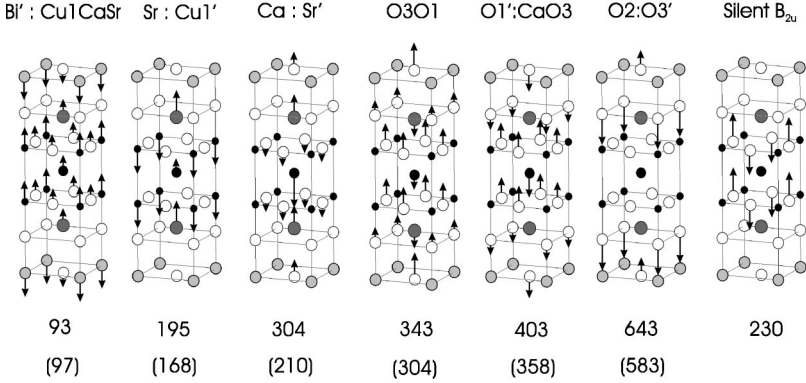


FIG. 7. Normal frequencies (in cm^{-1}) of six A_{2u} -symmetry modes and one “silent” B_{2u} mode in Bi2212 ($I4/mmm$) and schematic representation of their eigenvectors; respective experimental c -axis TO phonon frequencies are given in brackets (see Fig. 3 and Table VI).

topo effect in the Bi2212 single crystal, as investigated in this work (see Fig. 5). According to first-order perturbation theory, the frequency shift of the mode ω_n due to the change of the mass m_i of the i th atom is proportional to the square modulus of the i th component of the corresponding eigenvector^{46,47}:

$$\frac{\delta\omega_n}{\delta m_i} = -\frac{\omega_n}{2m_i} [|\xi_{i,x}|^2 + |\xi_{i,y}|^2 + |\xi_{i,z}|^2]. \quad (2)$$

In the experiment, a noticeable redshift upon ^{18}O substitution is observed for the three c -axis high-frequency modes. This result is consistent with our assignment that the

phonons at 304, 358, and 583 cm^{-1} have predominantly oxygen character; the calculated values of the isotope shifts based on the mode eigenvectors from Eq. (2) are 15.1, 15.1, and 33.8 cm^{-1} , respectively. The agreement between calculation and experiment is quite good. The low-frequency mode at 210 cm^{-1} also exhibits a noticeable redshift upon ^{18}O substitution. The calculated value of the isotope shift is 2.1 cm^{-1} . Although the quantitative agreement is not so good in this case, our assignment suggesting a noticeable contribution from the copper-plane O1 and bismuth-plane O3 atoms to this low-frequency mode is qualitatively consistent with the observed oxygen isotope effect. In addition, in agreement with the experiment our assignment suggests that

TABLE IX. Calculated components of eigenvectors of A_{2u} modes in Bi2201 ($\text{Bi}_2\text{Sr}_2\text{CuO}_6$), Bi2212 ($\text{Bi}_2\text{Sr}_2\text{CaCu}_2\text{O}_8$), and Bi2223 ($\text{Bi}_2\text{Sr}_2\text{Ca}_2\text{Cu}_3\text{O}_{10}$) crystals in tetragonal $I4/mmm$ (D_{4h}^{17}) space group.

Bi2212	Bi(z)	Sr(z)	Cu1(z)	–	Ca(z)	O1(z)	O2(z)	O3(z)	–
93 cm^{-1}	-0.46	0.27	0.33	–	0.29	0.16	-0.07	-0.11	–
195 cm^{-1}	-0.04	0.43	-0.54	–	0.16	0.05	-0.01	0.00	–
304 cm^{-1}	-0.09	0.33	0.10	–	-0.76	-0.15	0.08	0.18	–
343 cm^{-1}	-0.11	-0.18	-0.09	–	-0.15	0.31	0.13	0.46	–
403 cm^{-1}	0.09	-0.01	-0.04	–	-0.50	0.29	-0.15	-0.41	–
643 cm^{-1}	0.07	0.04	0.03	–	0.01	-0.01	-0.66	0.24	–
Bi2223	Bi(z)	Sr(z)	Cu1(z)	Cu2(z)	Ca(z)	O1(z)	O2(z)	O3(z)	O4(z)
88 cm^{-1}	-0.45	0.11	0.14	0.57	0.21	0.08	-0.07	-0.11	0.17
145 cm^{-1}	-0.23	0.33	0.22	-0.68	0.09	0.10	0.00	-0.01	-0.09
211 cm^{-1}	0.01	0.27	-0.59	-0.06	0.23	0.06	-0.03	0.00	0.09
252 cm^{-1}	-0.05	0.42	-0.05	0.29	-0.49	-0.07	0.02	0.03	-0.16
335 cm^{-1}	-0.09	-0.15	-0.07	-0.01	-0.21	0.29	0.10	0.46	0.16
378 cm^{-1}	0.10	-0.09	-0.05	0.09	-0.13	0.34	-0.14	-0.41	0.04
516 cm^{-1}	0.05	0.05	0.03	-0.21	-0.23	-0.05	-0.08	-0.22	0.60
666 cm^{-1}	0.08	0.03	0.05	0.00	0.01	-0.01	-0.66	0.22	0.02
Bi2201	Bi(z)	Sr(z)	Cu1(z)	–	–	O1(z)	O2(z)	O3(z)	–
77 cm^{-1}	-0.31	0.24	0.77	–	–	0.10	-0.11	-0.17	–
175 cm^{-1}	-0.21	0.51	-0.56	–	–	0.17	0.02	-0.06	–
293 cm^{-1}	-0.24	-0.09	0.08	–	–	0.30	0.15	0.56	–
353 cm^{-1}	0.10	-0.23	-0.08	–	–	0.59	-0.10	-0.27	–
596 cm^{-1}	0.09	0.06	-0.05	–	–	0.00	-0.66	0.23	–

Infrared A_{2u} (Bi2223 $I4/mmm$)

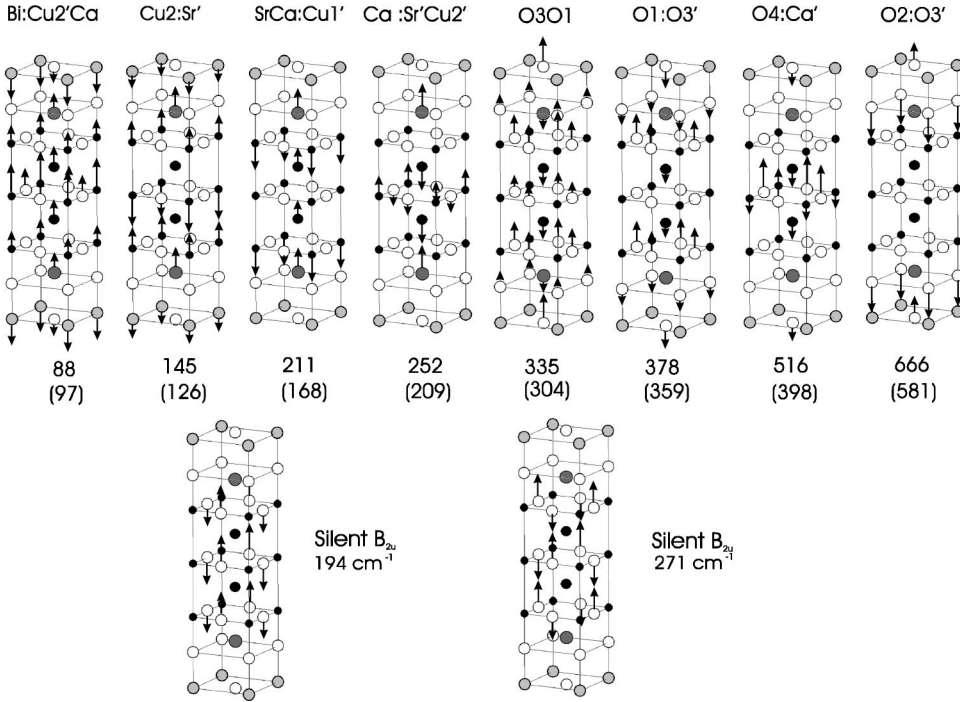


FIG. 8. Normal frequencies and eigenvectors of eight A_{2u} -symmetry modes and two “silent” B_{2u} modes in Bi2223 ($I4/mmm$); respective experimental c -axis TO phonon frequencies are given in brackets (see Fig. 3 and Table VI).

the next low-frequency mode at 195 cm^{-1} exhibits no oxygen isotope effect. The present shell model calculations thus reproduce the frequencies of the c -axis A_{2u} eigenmodes quite well for the bilayer Bi2212 single crystal. The observed oxygen isotope shifts of the phonon frequencies are consistent with the predictions based on the eigenvectors obtained from lattice-dynamical calculations, thus giving more confidence with our shell model parameters, normal-mode eigenvectors, and our assignment. We remark that although the eigenfrequencies are somewhat different, the character of A_{2u} vibrations resulting from the present shell model calculations for the Bi2212 system is consistent with the earlier calculations made by Prade *et al.*¹⁵

In Fig. 8 we show the eigenvector patterns corresponding to the eight eigenmodes of A_{2u} symmetry and two silent modes of B_{2u} symmetry for the Bi2223, resulting from our lattice-dynamical calculations with the same set of the shell model parameters listed in Table VII. The calculated components of the eigenvector amplitudes are summarized in Table IX. We make an assignment of the TO phonon modes observed in the c -axis ellipsometry spectra of the Bi2223 single crystal ($T=150\text{ K}$; see Fig. 3 and Table VI) based on a comparison with the present calculations. As can be seen from Figs. 7 and 8, a close similarity with the Bi2212 is observed for their eigenmode characters and eigenfrequency values due to the common generic features in the Bi2212 and Bi2223 structures. The only exception is that two new additional modes of A_{2u} symmetry are present for the trilayer Bi2223 system. Our calculations give one additional mode for Bi2223 at 145 cm^{-1} ; its character is defined by the main contribution from the Cu2 (from the inner CuO_2 plane) and Sr out-of-phase vibrations, and assigned it with the new mode clearly discernible in the $\epsilon_1(\omega)$ spectrum at 127 cm^{-1} [see Fig. 3(b)], which is also in agreement with the results of

IR measurements done very recently on an oriented ceramics of Bi2223 (Ref. 20). We calculated four A_{2u} “light,” predominantly oxygen-related, modes at the frequencies 335 , 378 , 516 , and 666 cm^{-1} . Like in the Bi2212, the highest-frequency mode at 666 cm^{-1} (581 cm^{-1}) is associated with the out-of-phase O2 and O3 vibrations, the mode calculated at 335 cm^{-1} (304 cm^{-1}) is predominantly due to the Bi-plane O3 oscillations, and the mode calculated at 378 cm^{-1} (359 cm^{-1}) is the Cu-O bond-bending character mode, corresponding to the out-of-phase motion of the Ca atoms and oxygens O1 in the outer CuO_2 planes. We calculated one additional oxygen-related mode in the Bi2223 at 516 cm^{-1} , and its character is defined by the out-of-phase vibrations of the Ca atoms and oxygens O4 in the inner CuO_2 plane. We assign it with the new mode appearing in the c -axis phonon spectrum of the Bi2223 at 402 cm^{-1} , as is clearly observable in Fig. 3, and also in agreement with the results of Ref. 20.

As we discussed in Sec. IV some of the c -polarized IR phonon modes in the bilayer Bi2212 and trilayer Bi2223 compounds exhibit a strongly anomalous temperature dependence at T_c , accompanied by the development of a sizable absorption peak below T_c in the FIR range, as illustrated in Fig. 6.^{2,5-7} The two most pronounced phonon bands at 304 and 582 cm^{-1} appear at the same frequencies in the c -axis ellipsometry spectra of the Bi2212 and Bi2223. According to our assignment they are associated with the predominant contribution from the BiO layer O3 oxygens and the apical O2 oxygens, respectively. It is evident from Fig. 6 that the formation of the t-JPR in Bi2212 and Bi2223 is accompanied by the strongly anomalous temperature dependence of the phonon modes at 360 , 402 (specific for trilayer Bi2223), and 582 cm^{-1} denoted by A, B, and C. An explanation of the anomalous changes of the phonon modes at 360 and

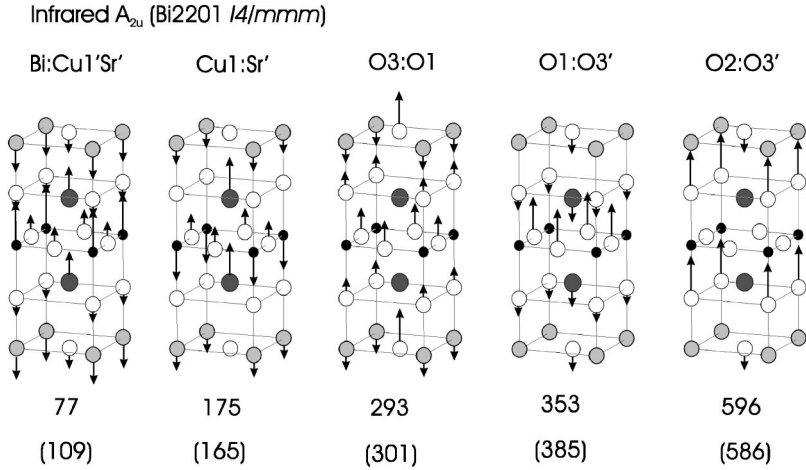


FIG. 9. Normal frequencies and eigenvectors of five A_{2u} -symmetry modes in Bi2201 ($I4/mmm$); experimental c -axis TO phonon frequencies are given in brackets (see Fig. 4 and Table VI).

402 cm^{-1} upon entering the superconducting state has been recently proposed based on the so-called Josephson superlattice model, assuming that these bands belong to the vibration of the planar oxygens.^{6,7} This assumption is supported by our assignment which suggests that these modes are bond-bending character modes which involve a significant contribution from the outer copper-plane O1 and inner copper-plane O4 ions, respectively.

In Fig. 9 we present the eigenvector pattern corresponding to the five eigenmodes of A_{2u} symmetry for Bi2201; the calculated components of the eigenvector amplitudes are listed in Table IX. We have calculated two A_{2u} symmetry modes at low frequencies. The calculated lowest-frequency mode is related to the motion of the heavy Bi atoms, which is strongly mixed with out-of-phase motion of Sr and Cu1. The next mode of A_{2u} symmetry is predominantly due to the motion of Cu1 against Sr. The three phonon features are clearly observed in the c -axis ellipsometry spectra of the Bi2201 at low frequencies at around 109, 165, and 209 cm^{-1} (see Fig. 4 and Table VI); in Sec. IV we have already discussed the possible reasons for the appearance of one “extra” phonon feature. We have made an assignment of the modes at low frequencies by analogy with the vibration characters at the corresponding frequencies in the B2212 and Bi2223 crystals. The three high-energy vibrations are predominantly oxygen related. The highest-frequency mode at 596 cm^{-1} (586 cm^{-1}) has apparently apical character due to the predominant contribution from the strontium-plane O2 oscillations along the c axis. The modes calculated at 293 cm^{-1} and 353 cm^{-1} are basically due to bismuth-plane O3 and copper-plane O1 mixed in-phase and out-of-phase vibrations, respectively, and they correlate well with the experimental frequencies at 301 and 385 cm^{-1} . In Bi2201 the CuO_2 planar oxygen band located at 385 cm^{-1} has much larger intensity than in Bi2212. This is probably due to the fact that in Bi2212 the CuO_2 planar oxygen mode is strongly renormalized by its coupling to interlayer electronic excitations already in the normal state.

The oscillator strengths of IR-active phonon modes are related to the dipole moment arising from the displacements of ions involved in a vibration:

$$S_j = \frac{4\pi}{V} \frac{\left[\sum_i e_{i_i}^* u_{ij} \right]^2}{\omega_{\text{TO}j}^2 \sum_i m_i u_{ij}^2} \quad (3)$$

In this relation V is the unit cell volume, $e_{i_i}^*$ and m_i correspond to the dynamical effective charge and mass of the i th atom vibrating in j mode with TO frequency $\omega_{\text{TO}j}$, and u_{ij} represents the displacements related to the eigenvector χ_j by $u_{ij} = \chi_{ij} / \sqrt{m_i}$. In most cases, however, the dynamical charges $e_{i_i}^*$ do not correspond to the static ionic ones. As we discussed earlier, to describe single-layer, bilayer, and trilayer Bi systems by the same set of potential parameters we have to keep the net ionic charges of the atoms in the cuprate planes of $+2|e|$ for Cu1 and Cu2 and $-2|e|$ for O1 and O4. Also in our model the effective charges of $-1.67|e|$ for O2 and O3 have been assumed. As an example, in Table X we present values of the oscillator strengths calculated from the displacements of ions, vibrating in the A_{2u} symmetry modes in Bi2212, using the ionic charges that were adopted in our shell model. As one can see, the qualitative agreement between model and experiment is quite good in the sense that the model correctly predicts the strongest modes in the phonon spectra and the weak modes are also predicted to be weak. An improved description of the oscillator strengths of all phonon modes compared to those with formal ionic charges can be achieved by introducing effective ionic charges. By inversion of Eq. (3) from the experimental oscillator strengths the effective charges of the ions can be extracted by making use of the calculated components of the eigenvectors. Following this procedure, in

TABLE X. Comparison of values of oscillator strengths calculated from components of eigenvectors of A_{2u} modes in Bi2212 with corresponding experimental values.

$\omega_{\text{TO}j}^{\text{expt}}$ (cm^{-1})	97	168	210	304	358	583
A_{2u} (cm^{-1})	93	195	304	343	403	643
S_j^{expt}	–	0.29	0.34	1.13	0.33	0.65
S_j^{calc}	0.07	0.16	0.03	4.24	0.11	0.13

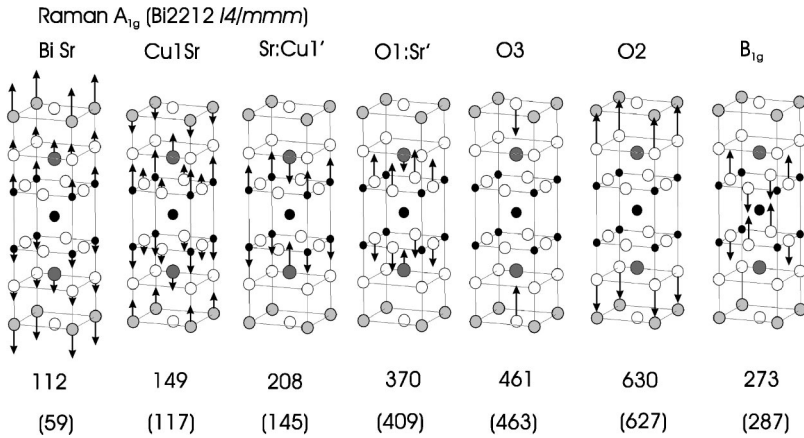


FIG. 10. Normal frequencies and eigenvectors of six A_{1g} -symmetry modes and one B_{1g} mode in Bi2212 ($I4/mmm$); experimental frequencies are given in brackets (Ref. 51).

general, we have arrived at the resulting charges close to the formal charges adopted within the model. The major improvement can be obtained if the O2 charge is made more negative and the O3 charge is made less negative, although a quantitative comparison seems to be in part uncertain, because, as we mention above, due to coupling to interlayer electronic excitations in multilayer Bi compounds the CuO_2 planar oxygen modes are strongly renormalized, already in the normal state. The consequences of these local field effects, which go beyond the scope of the present simple model, have been outlined in Refs. 2 and 6.

C. Calculated Γ -point A_{1g} -symmetry modes in Bi2201 , Bi2212 , and Bi2223

In this section we just briefly discuss the results of our shell model calculations for the Raman-active modes in the three Bi-based compounds and suggest an assignment for the phonon modes observed in the experimental spectra. It has been generally found that a larger number of phonon modes occur in the Raman spectra of the Bi-based compounds than would be expected from the simple tetragonal $I4/mmm$ symmetry consideration (given in Tables I and II). As a result different groups have reported rather different and then contradictory assignments. We have already referred to these reasons in Sec. II. There appears to be a consensus on the origin of the strong B_{1g} phonon in Raman spectra of Bi2212 . From the B_{1g} -symmetry selection rules the peak at about 285 cm^{-1} , which occurs only in the $z(xy)\bar{z}$ spectrum can be assigned to the O(1) B_{1g} phonon characterized by out-of-phase motion of the oxygen atoms in the CuO_2 plane. This is not the case, however, for two of the strongest A_{1g} modes that appear in the Raman spectrum at higher frequencies around 460 and 620 cm^{-1} . The origin of the high-frequency vibrations in the Raman spectrum of Bi2212 remains controversial despite many investigations by different groups. Most authors have assigned the 460-cm^{-1} mode to the vibrations of the apical oxygen atoms located in the SrO planes and the 620-cm^{-1} phonon to vibrations of the oxygen atoms located in the BiO planes.⁴⁸⁻⁵⁰ However, recently it was argued that the assignment should be reversed.^{51,52} It was shown that these two bands exhibit different polarization dependences for the incident and scattered vectors, indicating that the degree of mode mixing is small, and the 620-cm^{-1} band is

strongly c polarized like apex oxygen vibrations characteristic for most high- T_c superconductors.⁵¹ Moreover, the 460-cm^{-1} band has been found to soften at a significantly faster rate than the 620-cm^{-1} band with ^{18}O oxygen isotope substitution, in agreement with the more liable oxygen atoms from the BiO layer.⁵² Therefore, in fitting our shell model parameters for the Bi2212 crystal we have implied an assignment for the mode observed at around 285 cm^{-1} as the B_{1g} mode, whereas for the modes observed at around 460 and 620 cm^{-1} as the A_{1g} modes associated with the O3 (from the BiO plane) and O2 (from the SrO plane) predominant contributions, respectively.

In Fig. 10 we show our suggested eigenvector pattern corresponding to the six eigenmodes of A_{1g} symmetry and one B_{1g} symmetry for the Bi2212 crystal. We list values of the eigenfrequencies and below we make an assignment in agreement with the experimental Raman study of $\text{Bi}_2\text{Sr}_2\text{Ca}_{1-x}\text{Y}_x\text{Cu}_2\text{O}_{8+\delta}$ ($x=0-1$) single crystals.⁵¹ A number of phonons observable below 400 cm^{-1} in the Raman spectra in the A_{1g} (or A_g) scattering configurations are considered by Kakahana *et al.* as “disorder-induced” modes.⁵¹ In addition, as a weak satellite feature at $\sim 657\text{ cm}^{-1}$ near the strong phonon band at 620 cm^{-1} disappears in modulation-free $\text{Bi}_{2-x}\text{Pb}_x\text{Sr}_2\text{Ca}_{1-x}\text{Cu}_2\text{O}_{8+\delta}$ crystals it is possibly induced by the incommensurate superstructural modulation.⁵³ Another satellite feature at $\sim 458\text{ cm}^{-1}$ near the pronounced phonon band at 460 cm^{-1} is possibly associated with extra oxygen atoms in the BiO layers and also referred to “disorder-induced” scattering.

In Fig. 11 we show the eigenvector pattern corresponding to the seven eigenmodes of A_{1g} symmetry and one B_{1g} symmetry for the Bi2223 crystal, calculated using the same basic set of the shell model parameters. From Figs. 10 and 11 we can see that due to the common generic features in the Bi2212 and Bi2223 structures, the vibration characters are similar and the eigenfrequency values are close for the corresponding eigenmodes. This is consistent with the recently published results on Raman measurements showing that the frequencies of the major phonon bands are almost identical in Bi2212 and Bi2223 single crystals.⁵⁴ The exception is an additional mode of A_{1g} symmetry present in the trilayer Bi2223 crystal. Comparing the bilayer and trilayer systems (Figs. 10 and 11) we can conclude that instead of one A_{1g}

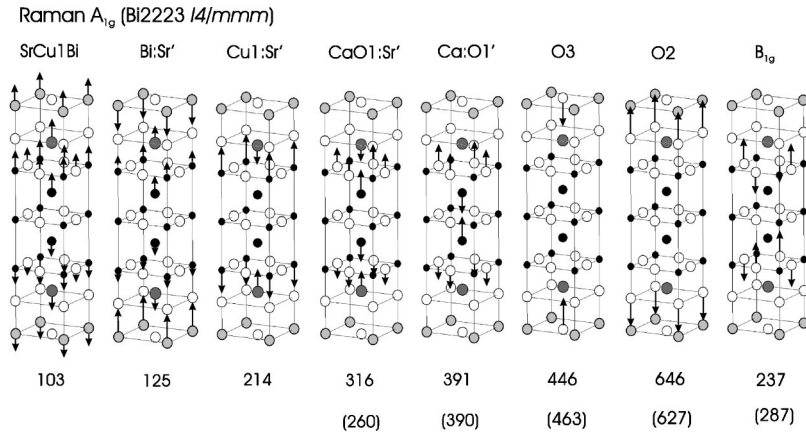


FIG. 11. Normal frequencies and eigenvectors of seven A_{1g} -symmetry modes and one B_{1g} mode in Bi2223 ($I4/mmm$); some experimental frequencies are given in brackets (see Fig. 13 and Ref. 54).

mode associated with the O1 vibrations in the CuO_2 plane in the Bi2212 structure, calculated at 370 cm^{-1} , in the Bi2223 structure we have two A_{1g} modes associated with the Ca and O1 (from the outer CuO_2 planes) in-phase and out-of-phase vibrations, calculated at 316 and 391 cm^{-1} , respectively.

In Fig. 12 we show the eigenvector pattern corresponding to the four eigenmodes of A_{1g} symmetry for the $I4/mmm$ Bi2201, resulting from our shell model calculations. As usual many more phonon modes are observed in the experimental Raman spectra, implying that the simple tetragonal approximation is no longer applicable for an interpretation of the Raman phonon spectra of the Bi2201. In Tables I and III we show that due to the orthorhombic distortions, the O1 atoms in the CuO_2 plane become “Raman active,” and as a result, a number of new Raman-active modes of A_g , B_{1g} , $2B_{2g}$, and $2B_{3g}$ character will appear in the *Amaa* Bi2201. We suggest that a more appropriate approximation for the interpretation of the Γ -point Raman-active phonons in this compound will be the orthorhombic *Amaa* space group. However, the assignment for the two high-frequency oxygen modes (as we show in Fig. 12) is the same as for the Bi2212 and Bi2223 crystals, and the calculated frequencies agree quite well for these three compounds.

Resonant Raman scattering below T_c has been discovered in Bi- and Hg-based high- T_c compounds with three or four CuO_2 layers.^{54–56} Strong superconductivity-induced en-

hancement of the phonons at 260 and 390 cm^{-1} , together with the development of a broadband peaking at around 580 cm^{-1} , has been observed in a recent resonant Raman scattering study on the Bi2223 single crystal with $T_c = 109 \text{ K}$ (Ref. 54). Our measurements of resonant Raman scattering ($E_{exc} = 2.18 \text{ eV}$) done on our Bi2223 single crystal with lower $T_c = 107 \text{ K}$ reproduce the results of Limonov *et al.* In Fig. 13(a) we show the Raman spectra at two different temperatures—i.e., somewhat above and well below T_c . Figure 13(b) shows the difference between these Raman spectra. Our data clearly demonstrate the superconductivity-induced enhancement of the phonon bands at 260 and 390 cm^{-1} and a broadband peaking around 550 cm^{-1} .

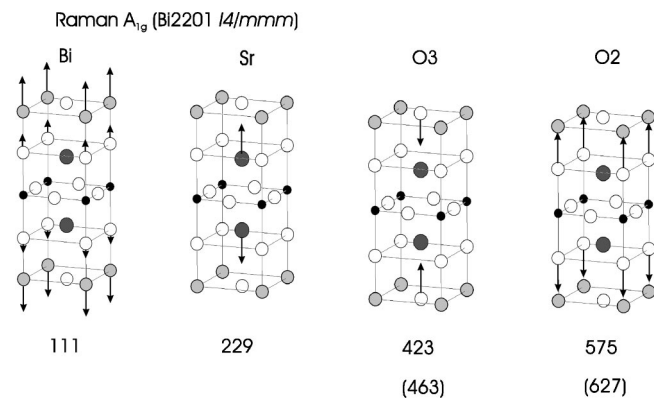


FIG. 12. Normal frequencies and eigenvectors of four A_{1g} -symmetry modes in Bi2201 ($I4/mmm$); some experimental frequencies are given in brackets (Ref. 51).

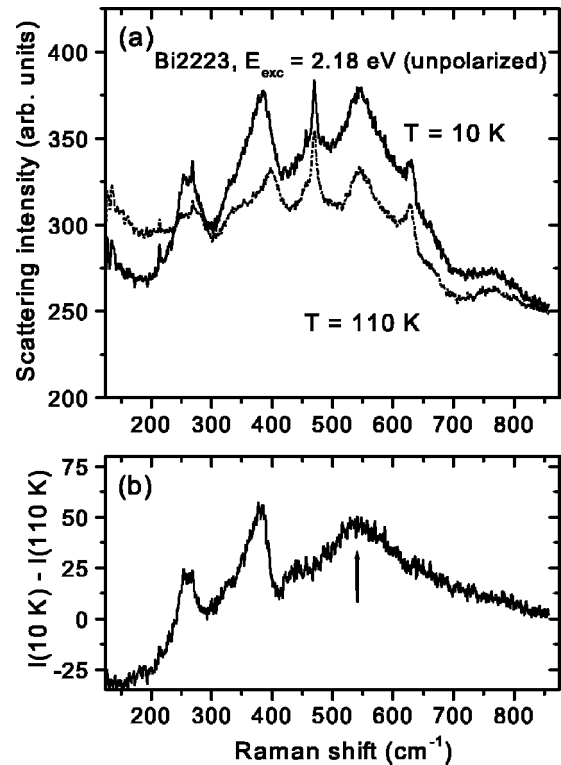


FIG. 13. Raman scattering ($E_{exc} = 2.18 \text{ eV}$) in Bi2223 (a) measured slightly above $T_c = 107 \text{ K}$ and well below T_c and (b) resonant enhancement of the phonon bands at 260 and 390 cm^{-1} and superconductivity-induced broadband at 550 cm^{-1} .

There are two alternative explanations of these superconductivity-induced anomalies in multilayer high- T_c compounds; one considers the broad excitation band as a “pair-breaking” peak at 2Δ (Ref. 54) and the other refers to it as a Raman-active c axis plasmon.⁵⁶ A more detailed study of the doping effect on the resonance peak position is required to clarify its origin. Nevertheless, discussing the phonon anomalies observed in trilayer Bi2223 we would like to notice that both approaches consider the superconductivity-induced anomalies as due to strong coupling of the intralayer electronic excitation with phonons which involve calcium and planar oxygen ions. Experimental resonant Raman scattering studies bring evidence in favor of our assignment suggested for the trilayer Bi2223 crystal (Fig. 11). The superconductivity-enhanced phonon bands at 260 and 390 cm^{-1} in the Bi2223 can be ascribed to the A_{1g} in-phase and out-of-phase vibrations of the Ca atoms with oxygens in the outer CuO_2 planes, in agreement with our assignment for the A_{1g} modes calculated at 316 and 391 cm^{-1} .

VI. CONCLUSIONS

In summary, we present experimental data on single crystals as obtained by spectral ellipsometry and make the assignment of the IR c -axis-polarized phonon modes in single-layer, bilayer, and trilayer bismuth compounds (Bi2201, Bi2212, and Bi2223) by comparing them with the results of the shell model calculations. The c -axis IR phonon spectra look very similar for the bilayer and trilayer Bi-based crystals, supporting experimental evidence for the generic structural features of these compounds. We apply a tetragonal $I4/mmm$ approximation in the interpretation of the c -axis IR spectra of the Bi-based compounds, which are known to have pseudotetragonal structure, and conclude that this approximation provides a reasonable description of the main features in the phonon spectra. In the framework of this approximation, we have identified “disorder-induced” modes due to the orthorhombic distortions associated with the incommensurate superstructural modulations and extra-stoichiometric oxygen. Comparing with the bilayer Bi system, we identify two additional c -axis phonon modes in the

ellipsometric spectra of the trilayer system: one at 127 cm^{-1} , among the “heavy” modes, and the other at 402 cm^{-1} , among the “light” modes, which according to our assignment involve a significant contribution of the copper and oxygen atoms in the inner CuO_2 plane, respectively. The recent experimental observation of a Josephson-plasma resonance and phonon anomalies in Bi2223 (Ref. 7) provides, indeed, strong support for the Josephson-superlattice model, which consistently explains the phonon anomalies and the formation of a broad absorption band below T_c using components of the eigenvector amplitudes for the relevant oxygen modes at 358 and 402 cm^{-1} . The two modes involving O3 (BiO plane) and O1 (CuO_2 plane) atoms exhibit substantial frequency changes in the single-layer system and appear at 294 and 389 cm^{-1} , respectively. For the single-layer system the mode at 389 cm^{-1} increases dramatically in intensity. This evident difference between single-layer and multilayer compounds in the behavior of this particular phonon mode reflects the fact that in multilayer compounds the oxygen bond-bending phonon mode is strongly coupled with the electronic excitation due to the charge density oscillations between the closely spaced CuO_2 planes. In addition, we also show the eigenvector patterns and calculated frequencies for the Raman-active phonon modes of A_{1g} symmetry in these three compounds according to the results of the present shell model calculations. The superconductivity-induced resonant Raman scattering for the two phonon modes at 260 and 390 cm^{-1} very recently observed in trilayer Bi2223 single crystal⁵⁴ is well consistent with the suggested assignment.

ACKNOWLEDGMENTS

The authors thank J. Gale for making available general utility lattice program (GULP) used in the present calculations. We are grateful to R. Evarestov and E. Kotomin for fruitful discussions. T.H. acknowledges support by the AvH Foundation. We acknowledge L. Carr at NSLS and Y.-L. Mathis at ANKA for their support during the ellipsometry measurements.

*Also at the Institute for Solid State Physics, Russian Academy of Sciences, Chernogolovka, Moscow distr. 142432, Russia.

¹M. Grüninger, D. van der Marel, A.A. Tsvetkov, and A. Erb, Phys. Rev. Lett. **84**, 1575 (2000).

²D. Munzar, C. Bernhard, A. Golnik, J. Humlíček, and M. Cardona, Solid State Commun. **112**, 365 (1999).

³D. van der Marel and A.A. Tsvetkov, Phys. Rev. B **64**, 024530 (2001).

⁴C. Bernhard, D. Munzar, A. Golnik, C.T. Lin, A. Wittlin, J. Humlíček, and M. Cardona, Phys. Rev. B **61**, 618 (2000).

⁵V. Železný, S. Tajima, T. Motohashi, J. Shimoyama, K. Kishio, and D. van der Marel, J. Low Temp. Phys. **117**, 1019 (1999); V. Železný, S. Tajima, D. Munzar, T. Motohashi, J. Shimoyama, and K. Kishio, Phys. Rev. B **63**, 060502 (2001).

⁶D. Munzar, C. Bernhard, T. Holden, A. Golnik, J. Humlíček, and M. Cardona, Phys. Rev. B **64**, 024523 (2001).

⁷A.V. Boris, D. Munzar, N.N. Kovaleva, B. Liang, C.T. Lin, A. Dubroka, A.V. Pimenov, T. Holden, B. Keimer, Y.-L. Mattis, and C. Bernhard, Phys. Rev. Lett. **89**, 277001 (2002).

⁸W. Kress and U. Shróder, Phys. Rev. B **38**, 2906 (1988).

⁹R. Liu, C. Thomsen, W. Kress, M. Cardona, B. Gegenheimer, F.W. Wette, J. Prade, A.D. Kulkarni, and U. Shróder, Phys. Rev. B **37**, 7971 (1988).

¹⁰J. Humlíček, A.P. Litvinchuk, W. Kress, B. Lederle, C. Thomsen, M. Cardona, H.-U. Habermeier, I.E. Trofimov, and W. König, Physica C **206**, 345 (1993).

¹¹T. Timusk, C.C. Homes, and W. Reichardt, in *International Workshop on the Anharmonic Properties of High T_c Cuprates, Bled, Slovenia, 1994*, edited by G. Ruani (World Scientific, Singapore, 1995).

¹²R. Henn, T. Strach, E. Schönher, and M. Cardona, Phys. Rev. B **55**, 3285 (1997).

- ¹³S. Tajima, G.D. Gu, S. Miyamoto, A. Odagawa, and N. Koshizuka, *Phys. Rev. B* **48**, 16164 (1993).
- ¹⁴A.A. Tsvetkov, D. Dulic, D. van der Marel, A. Damascelli, G.A. Kaljushnaia, J.I. Gorina, N.N. Senturina, N.N. Kolesnikov, Z.F. Ren, J.H. Wang, A.A. Menovsky, and T.T.M. Palstra, *Phys. Rev. B* **60**, 13196 (1999).
- ¹⁵J. Prade, A.D. Kulkarni, F.W. de Wette, U. Schroder, and W. Kress, *Phys. Rev. B* **39**, 2771 (1989).
- ¹⁶Chun-Sheng Jia, Pi-Yuan Lin, Yang Xiao, Xiao-Wei Jiang, Xue-Yan Gou, Su Huo, Hao Li, and Qiu-Bo Yang, *Physica C* **268**, 41 (1996).
- ¹⁷Sheng Jia Chun and Shu Zhou Wu, *Phys. Status Solidi B* **163**, K49 (1991).
- ¹⁸A.D. Kulkarni, F.W. de Wette, J. Prade, U. Schroder, and W. Kress, *Phys. Rev. B* **41**, 6409 (1990).
- ¹⁹T. Zetterer, M. Franz, J. Schützmann, W. Ose, H.H. Otto, and K.F. Renk, *Phys. Rev. B* **41**, 9499 (1990).
- ²⁰N. Petit, V. Garnier, V. Ta Phuoc, R. Caillard, A.-M. Frelin, A. Ruyter, I. Laffez, J.-C. Soret, A. Maignan, and F. Gervais, *Eur. Phys. J. B* **25**, 423 (2002).
- ²¹B. Liang, C.T. Lin, P. Shang, and G. Yang, *Physica C* **383**, 75 (2002).
- ²²B. Liang and C.T. Lin, *J. Cryst. Growth* **237-239**, 756 (2002); B. Liang, C.T. Lin, A. Maljuk, and Y. Yan, *Physica C* **366**, 254 (2002).
- ²³B. Liang, A. Maljuk, and C.T. Lin, *Physica C* **361**, 156 (2001); C.T. Lin, B. Liang, M. Freiberg, K. Peters, and E. Schoenher, *ibid.* **341**, 541 (2000).
- ²⁴A.M. Stoneham and L.W. Smith, *J. Phys.: Condens. Matter* **3**, 225 (1991).
- ²⁵S.L. Chaplot, W. Reichardt, L. Pintschovius, and N. Pyka, *Phys. Rev. B* **52**, 7230 (1995).
- ²⁶R.C. Baetzold, *Phys. Rev. B* **38**, 11304 (1988).
- ²⁷M.S. Islam, M. Leslie, S.M. Tomlinson, and C.R.A. Catlow, *J. Phys. C* **21**, L109 (1988).
- ²⁸J.D. Gale, *Philos. Mag. B* **73**, 3 (1996); *J. Chem. Soc., Faraday Trans.* **93**, 629 (1997).
- ²⁹J.M. Tarascon, Y. Le Page, P. Barboux, B.G. Bagley, L.H. Greene, W.R. McKinnon, G.W. Hull, M. Giroud, and D.M. Hwang, *Phys. Rev. B* **37**, 9382 (1988).
- ³⁰J.M. Tarascon, Y. Le Page, P. Barboux, B.G. Bagley, L.H. Greene, W.R. McKinnon, G.W. Hull, M. Giroud, and D.M. Hwang, *Phys. Rev. B* **38**, 8885 (1988).
- ³¹K. Imai, T. Kawashima, S. Sueno, and A. Ono, *Jpn. J. Appl. Phys., Part 2* **27**, L1661 (1988).
- ³²C.C. Torardi, M.A. Subramanian, J.C. Calabrese, J. Gopalakrishnan, E.M. McCarron, K.J. Morrissey, T.R. Askew, R.B. Flippen, U. Chowdhry, and A.W. Sleight, *Phys. Rev. B* **38**, 225 (1988).
- ³³A. Sequeira, H. Rajagopal, P.V.P.S.S. Sastry, J.V. Yakhmi, and R.M. Iyer, *Physica B* **174**, 367 (1991).
- ³⁴Y. Ito, A.-M. Vlaicu, T. Mukoyama, S. Sato, S. Yoshikado, C. Julien, I. Chong, Y. Ikeda, M. Takano, and E.Ya. Sherman, *Phys. Rev. B* **58**, 2851 (1998).
- ³⁵P. Bordet, J.J. Capponi, C. Chaillout, J. Chenavas, A.W. Hewat, E.A. Hewat, J.L. Hodeau, M. Marezio, J.L. Tholence, and D. Tranqui, *Physica C* **156**, 189 (1988).
- ³⁶E. Bellingeri, G. Grasso, R.E. Gladyshevskii, M. Dhalles, and R. Flükiger, *Physica C* **329**, 267 (2000).
- ³⁷N. Jacubowicz, D. Grebille, M. Hervieu, and H. Leligny, *Phys. Rev. B* **63**, 214511 (2001) and references therein.
- ³⁸D.J. Pringle, *Phys. Rev. B* **62**, 12527 (2000).
- ³⁹R. Henn, C. Bernhard, A. Wittlin, M. Cardona, and S. Uchida, *Thin Solid Films* **313-314**, 643 (1998).
- ⁴⁰A.V. Boris (unpublished).
- ⁴¹C.C. Homes, A.W. McConnell, B.P. Clayman, D.A. Bonn, Ruixing Liang, W.N. Hardy, M. Inoue, H. Negishi, P. Fournier, and R.L. Greene, *Phys. Rev. Lett.* **84**, 5391 (2000).
- ⁴²C.R.A. Catlow and A.M. Stoneham, *J. Phys. C* **16**, 4321 (1983).
- ⁴³C.R.A. Catlow, W.C. Mackrodt, M.J. Norgett, and A.M. Stoneham, *Philos. Mag.* **35**, 177 (1977).
- ⁴⁴V.N. Popov, *J. Phys.: Condens. Matter* **7**, 625 (1995).
- ⁴⁵Our earlier fit of the shell model parameters was based on the experimental data only of the *c*-axis IR phonons. Although these earlier calculations resulted, in principle, in the same assignment and character of the A_{2u} modes as the present calculations, we arrived at somewhat different eigenvalues of the A_{2u} modes, in particular for the Bi2223 presented in Ref. 7.
- ⁴⁶A. Debernardi and M. Cardona, *Phys. Rev. B* **54**, 11 305 (1996).
- ⁴⁷J. Menéndez, J.B. Page, and S. Guha, *Philos. Mag. B* **70**, 651 (1994).
- ⁴⁸M. Cardona, C. Thomsen, R. Liu, H.G. von Schnering, M. Hartweg, Y.F. Yan, and Z.X. Zhao, *Solid State Commun.* **66**, 1255 (1988).
- ⁴⁹R. Liu, M.V. Klein, P.D. Han, and D.A. Payne, *Phys. Rev. B* **45**, 7392 (1992).
- ⁵⁰M. Boekholt, A. Erle, P.C. Splitterger-Hunnekes, and G. Guntherodt, *Solid State Commun.* **74**, 1107 (1990).
- ⁵¹M. Kakihana, M. Osada, M. Käll, L. Börjesson, H. Mazaki, H. Yasuoka, M. Yashima, and M. Yoshimura, *Phys. Rev. B* **53**, 11796 (1996).
- ⁵²A.E. Pantoya, D.M. Pooke, H.J. Trodahl, and J.C. Irwin, *Phys. Rev. B* **58**, 5219 (1998).
- ⁵³L. Ben-Dor, M.Y. Szerer, G. Blumberg, A. Givan, L. Börjesson, and L.V. Hong, *Physica C* **200**, 418 (1992).
- ⁵⁴Michail Limonov, Sergey Lee, and Setsuko Tajima, *Phys. Rev. B* **66**, 054509 (2002).
- ⁵⁵V.G. Hadjiev, Xingjiang Zhou, T. Strohm, M. Cardona, Q.M. Lin, and C.W. Chu, *Phys. Rev. B* **58**, 1043 (1998).
- ⁵⁶D. Munzar and M. Cardona, *Phys. Rev. Lett.* **90**, 077001 (2003).